Modelling a star

Project 2, AST3310
Spring 2019

Jowita Borowska

1 Introduction

The numerical model created in the first project is now being expanded by including the energy transport through convection. All the assumptions made before still hold (fully ionized, ideal gas; energy produced entirely as a result of Proton-Proton chain reactions; as well as the fact that mass fractions of each atomic species are known and constant). Moreover, we assume no heat conduction, so that the energy is transported exclusively by radiation and convection.

The goal is modelling a star whose luminosity, mass and radius converge within the range of $0 - 5\%$ of their initial values, in addition to the core ($L < 0.995L_0$) reaching out to at least 10% of the initial radius and continuous convection zone near the surface of the star with width at least 15% of the initial radius. Furthermore, we want the energy production from the PPI branch to be dominating at low temperatures and PPII, PPIII dominating at higher temperatures (closer to the center of the star). We are about to integrate our way from the surface toward the center of the star, varying values of some initial parameters (radius, density, temperature and pressure) with the purpose of finding the best-fit ones, fulfilling the mentioned goals.

2 Method

2.1 Equations governing the energy transport in a star

The total energy flux is given by

$$F = F_R + F_C = \frac{16\sigma T^4}{3\kappa\rho H_p}\nabla_{stable}, \tag{1}$$

where F_R, F_C are consecutively radiative and convective fluxes, σ is Stefan-Boltzmann constant, T is temperature, κ is opacity (read from the file by interpolation/extrapolation), ρ is density, ∇_{stable} is the temperature gradient needed for all the energy to be carried by radiation

and H_p is the pressure scale height, which in a static atmosphere (where gravity and pressure are in balance) for an ideal gas is equal to

$$H_p = \frac{k_B T}{\mu m_u g},$$

where k_B is Boltzmann constant, μ is average atomic weight of the particles, m_u is atomic mass unit and g is gravitational acceleration, $g = \frac{GM}{R(M)^2}$.
Furthermore, the radiative flux can be expressed as

$$F_R = \frac{16\sigma T^4}{3\kappa\rho H_p}\nabla^*, \tag{2}$$

where ∇^* is now the actual temperature gradient. The expression for convective flux is

$$F_C = \rho c_p T\sqrt{g\delta}H_p^{-\frac{3}{2}}\left(\frac{l_m}{2}\right)^2(\nabla^* - \nabla_p)^{\frac{3}{2}}, \tag{3}$$

where c_p is the specific heat at constant pressure, for a monoatomic ideal gas equal $c_p = \frac{5}{2}nk_B = \frac{5}{2}R$ (n being the number density of atoms and R - gas constant). Moreover, δ is a parameter that can be shown to be 1 for an ideal gas, $l_m = \alpha H_p$ is the mixing length, where α ia a parameter assumed to be equal 1 throughout the project, and ∇_p is the temperature gradient associated with the rising parcel of gas.

Now, inserting formulas (2) and (3) into equation (1), we get

$$\frac{16\sigma T^4}{3\kappa\rho H_p}\nabla^* + \rho c_p T\sqrt{g\delta}H_p^{-\frac{3}{2}}\left(\frac{l_m}{2}\right)^2(\nabla^* - \nabla_p)^{\frac{3}{2}} = \frac{16\sigma T^4}{3\kappa\rho H_p}\nabla_{stable},$$

$$(\nabla^* - \nabla_p)^{\frac{3}{2}} = \frac{\frac{16\sigma T^3\sqrt{H_p}}{3\kappa\rho}(\nabla_{stable} - \nabla^*)}{\rho c_p\sqrt{g\delta}\left(\frac{l_m}{2}\right)^2},$$

$$(\nabla^* - \nabla_p)^{\frac{3}{2}} = \frac{64\sigma T^3\sqrt{H_p}(\nabla_{stable} - \nabla^*)}{3\kappa\rho^2 c_p l_m^2\sqrt{g\delta}},$$

which inserting the formula for H_p becomes

$$(\nabla^* - \nabla_p) = \left(\frac{64\sigma T^{\frac{7}{2}}\sqrt{k_B}(\nabla_{stable} - \nabla^*)}{3g\sqrt{\mu m_u\delta}\kappa\rho^2 c_p l_m^2}\right)^{\frac{2}{3}}, \tag{4}$$

being the solution to Exercise 5.11.

Furthermore, we have the following equation

$$(\nabla_p - \nabla_{ad}) = \frac{32\sigma T^3}{3\kappa\rho^2 c_p v}\frac{S}{Qd}(\nabla^* - \nabla_p),$$

where ∇_{ad} is the adiabatic temperature gradient, $\frac{S}{Qd}$ is the geometric factor equal to $\frac{2}{r_p} = \frac{4}{l_m}$ for a spherical parcel with radius r_p, and v is the velocity given by

$$v = \sqrt{\frac{g\delta l_m^2}{4H_p}}(\nabla^* - \nabla_p)^{\frac{1}{2}}. \tag{5}$$

By inserting the veolocity expression into the equation above and using the relation: $(\nabla_p - \nabla_{ad}) = (\nabla^* - \nabla_{ad}) - (\nabla^* - \nabla_p)$, we get the second order equation for $\xi = (\nabla^* - \nabla_p)^{\frac{1}{2}}$:

$$(\nabla^* - \nabla_{ad}) - (\nabla^* - \nabla_p) = \frac{32\sigma T^3}{3\kappa\rho^2 c_p}\frac{S}{Qd}\sqrt{\frac{4H_p}{g\delta l_m^2}}(\nabla^* - \nabla_p)^{\frac{1}{2}},$$

$$(\nabla^* - \nabla_{ad}) - (\nabla^* - \nabla_p) = \frac{64\sigma T^3}{3\kappa\rho^2 c_p}\frac{S}{l_m Qd}\sqrt{\frac{H_p}{g\delta}}(\nabla^* - \nabla_p)^{\frac{1}{2}},$$

$$(\nabla^* - \nabla_{ad}) - (\nabla^* - \nabla_p) = \frac{S}{l_m Qd}U(\nabla^* - \nabla_p)^{\frac{1}{2}},$$

where

$$U = \frac{64\sigma T^3}{3\kappa\rho^2 c_p}\sqrt{\frac{H_p}{g\delta}}$$

has been used. Proceeding with the calculation we get

$$0 = (\nabla^* - \nabla_p) + \frac{US}{l_m Qd}(\nabla^* - \nabla_p)^{\frac{1}{2}} - (\nabla^* - \nabla_{ad}),$$

$$0 = \xi^2 + \frac{US}{l_m Qd}\xi - (\nabla^* - \nabla_{ad}),$$

which mathematically has the solutions:

$$\xi = \frac{-\frac{US}{l_m Qd} \pm \sqrt{\left(\frac{US}{l_m Qd}\right)^2 + 4(\nabla^* - \nabla_{ad})}}{2} = -\frac{US}{2l_m Qd} \pm \sqrt{\left(\frac{US}{2l_m Qd}\right)^2 + (\nabla^* - \nabla_{ad})}.$$

Nevertheless, as all the temperature gradients are positive and criterion

$$\nabla_{stable} > \nabla^* > \nabla_p > \nabla_{ad}$$

needs to be fulfilled, we have that $(\nabla^* - \nabla_{ad}) > 0$, as well as $\xi^2 = (\nabla^* - \nabla_p) > 0$. The only viable solution is then the one with the '+' sign, so that

$$\xi = -\frac{US}{2l_m Qd} + \sqrt{\left(\frac{US}{2l_m Qd}\right)^2 + (\nabla^* - \nabla_{ad})}, \tag{6}$$

being the solution to Exercise 5.12.

Now, rewriting the equation (4), using ξ and U defined as before, we get

$$\xi^3 = \frac{U}{l_m^2}(\nabla_{stable} - \nabla^*),$$

and from the derivation of ξ:

$$0 = \xi^2 + \frac{US}{l_m Qd}\xi - (\nabla^* - \nabla_{ad}) \Rightarrow \nabla^* = \xi^2 + \frac{US}{l_m Qd}\xi + \nabla_{ad}.$$

Combining these two expressions, we get

$$0 = \frac{l_m^2}{U}\xi^3 + \xi^2 + \frac{US}{l_m Qd}\xi + (\nabla_{ad} - \nabla_{stable}), \tag{7}$$

being the solution to Exercise 5.13. This equation can be further solved inserting $\frac{S}{Qd} = \frac{4}{l_m}$ and $l_m = \alpha H_p$.

2.2 Including convection - alterations in the algrotihm and program

The program written for the first project solves numerically partial differential equations with mass as the independent variable. We follow the same algorithm as before, but in order to include energy transport by convection, we adapt the program to check the convective instability at each mass shell, altering the expression for $\frac{\partial T}{\partial m}$. We derive the following relation:

$$\nabla = -\frac{H_p}{T}\frac{\partial T}{\partial r} \Rightarrow \nabla\frac{\partial r}{\partial m} = -\frac{H_p}{T}\frac{\partial T}{\partial r}\frac{\partial r}{\partial m} \Rightarrow \frac{\partial T}{\partial m} = -\frac{T}{H_p}\nabla\frac{\partial r}{\partial m},$$

where $\frac{\partial r}{\partial m} = \frac{1}{4\pi r^2\rho}$, as defined in project one. Temperature gradient that we use in the formula above depends on the convective stability check, so that

$$\nabla = \begin{cases} \nabla^* = \xi^2 + \frac{4U}{\alpha^2 H_p^2}\xi + \nabla_{ad} & \text{for } \nabla_{stable} > \nabla_{ad} \text{ (convective instability)}, \\ \nabla^* = \nabla_{stable} = \frac{3\kappa H_p \rho L}{64\pi\sigma r^2 T^4} & \text{otherwise (convective stability).} \end{cases} \tag{8}$$

Formula for calculating ∇^* has already been derived, we use numpy.roots to solve the cubic equation involving ξ (7) and subsequently choose the real solution from the three roots (as $\xi = \sqrt{\nabla^* - \nabla_p}$, the real solution will be positive).
We have obtained formula for ∇_{stable} by using the fact that the total energy flux, F, given by formula (1) is equal $\frac{L}{4\pi r^2}$. Moreover, ∇_{ad} is constant and for monoatomic ideal gas equal $2\alpha/(5\delta)$, which is simply 0.4 here.

In each step, after the differential equations are solved (using Euler's method), the next value of opacity, κ, is being read from the file by performing linear 2D interpolation/extrapolation. Thereafter, the next density is being computed, followed by calculation of the full energy generation per unit mass through PP-chain reactions, ε, as well as the energy produced by each of the three branches separately. Then, ∇_{stable} and ∇^* are being computed, where ∇^* depends on the agreement with instability criterion, obeying formula (8). Finally, radiative flux is being calculated using formula (2), as well as the convective flux - subtracting F_R from expression (1) (moreover, dividing each by the sum, $F = F_R + F_C$, we get the fractions of energy being transported by radiation and convection).

Tests of the formulas, algorithm and numerical implementation were performed with use of the available *sanity checks*. Both tests - the values provided by example 5.1, as well as the plots of ∇s and cross section - seem to be in agreement with the results produced by the program.

3 Results

3.1 Impact of initial parameters on width of the convection zone

The initial parameters, we begin with, are in agreement with the actual values of the solar surface: $L_0 = L_\odot$, $R_0 = R_\odot$, $M_0 = M_\odot$, $T_0 = T_{\odot,S} = 5770$ K, $\rho_0 = \rho_{\odot,S} = 1.42 \cdot 10^{-7} \cdot \overline{\rho}_\odot$ (where $\overline{\rho}_\odot$ is the average density of the Sun). In order to fulfill the goals mentioned in the *Introduction*, we may change the values of initial radius and temperature by a factor of 5, as well as initial density, that can be changed freely.

Many tests have been conducted, in order to investigate the impact that initial parameters have on width of the convection zone. We are changing the value of only one initial parameter at a time, leaving the other two, we are looking for, unchanged. This strategy is somehow

limited by the possibility of numerical problems that may occur for some combinations of parameters. The following plots show the tendencies of size of the outer convection layer during careful alterations of initial parameters. The horizontal line on ∇s-plots represents the adiabatic temperature gradient, that is constant in time. If the plotted temperature gradient is above that level ($\nabla_{stable} > \nabla_{ad}$), we are in the convection layer, otherwise we have the energy transport only by radiation (where $\nabla^* = \nabla_{stable} < \nabla_{ad}$). Plots of the cross section of the star, with outer convection layer marked in red, are also included for our initial density analysis, as it shows the clearest tendency to change.

- Test of the initial values of **density**, ρ_0: $\rho_{\odot,S}$ with width of the outer convection layer equal 0.97% of R_0, $10\rho_{\odot,S}$ with the width 7.10% of R_0 and $0.5\rho_{\odot,S}$ with the width 0.68% of R_0.

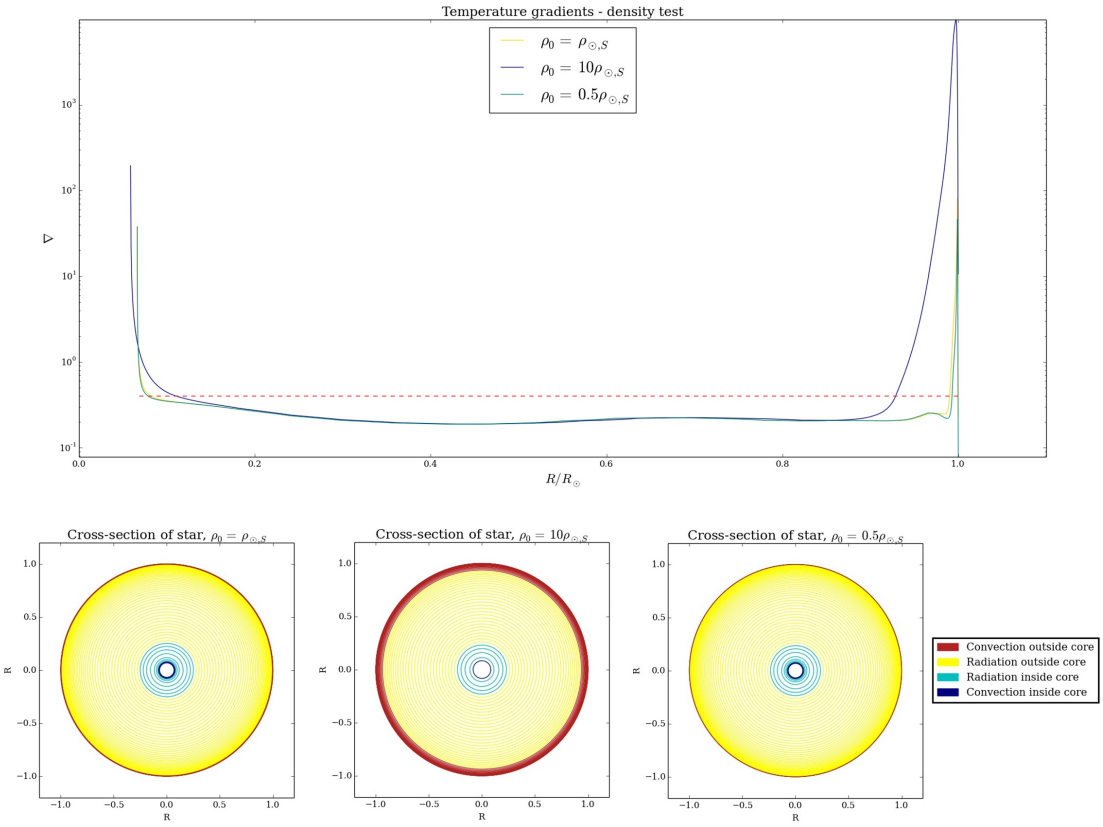

Figure 1: Test of the initial values of density, equal $\rho_{\odot,S}$, $10\rho_{\odot,S}$, $0.5\rho_{\odot,S}$ (where $\rho_{\odot,S}$ is the density of the solar surface). Upper plot shows the temperature gradients (dashed line: ∇_{ad}, solid line: ∇_{stable}) and lower - cross sections of stars corresponding to the given initial parameters.

- Test of the initial values of **temperature**, T_0: $T_{\odot,S}$ with width of the outer convection layer equal 0.97% of R_0, 1.4 $T_{\odot,S}$ with the width 0.76% of R_0 and 0.8 $T_{\odot,S}$ with the width 1.31% of R_0.

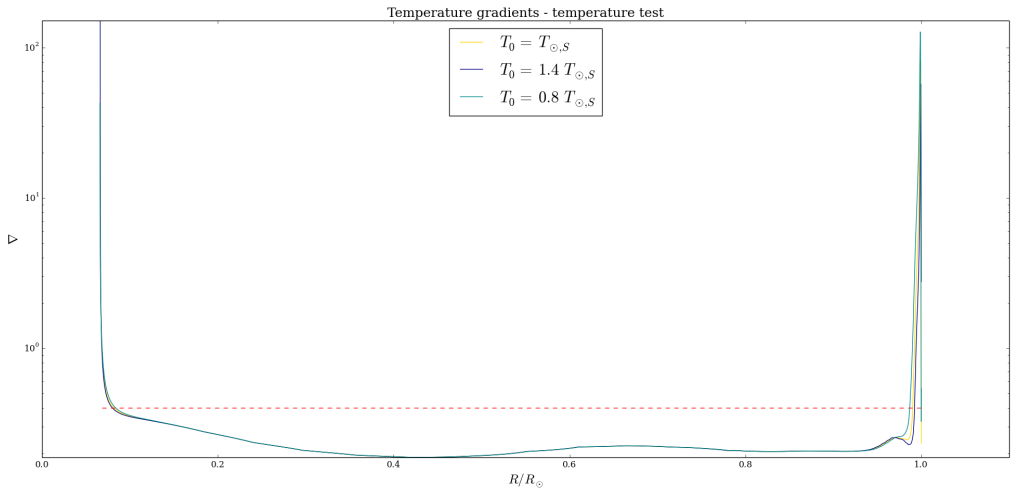

Figure 2: Test of the initial values of temperature, equal $T_{\odot,S}$, 1.4 $T_{\odot,S}$, 0.8 $T_{\odot,S}$ (where $T_{\odot,S}$ is the temperature of the solar surface $\approx$ 5770 K). Plot shows the temperature gradients (dashed line: ∇_{ad}, solid line: ∇_{stable}).

- Test of the initial values of **radius**, R_0: $R_\odot$ with width of the outer convection layer equal 0.97% of R_0, 1.1 $R_\odot$ with the width 1.21% of R_0 and 0.99 $R_\odot$ with the width 0.95% of R_0.

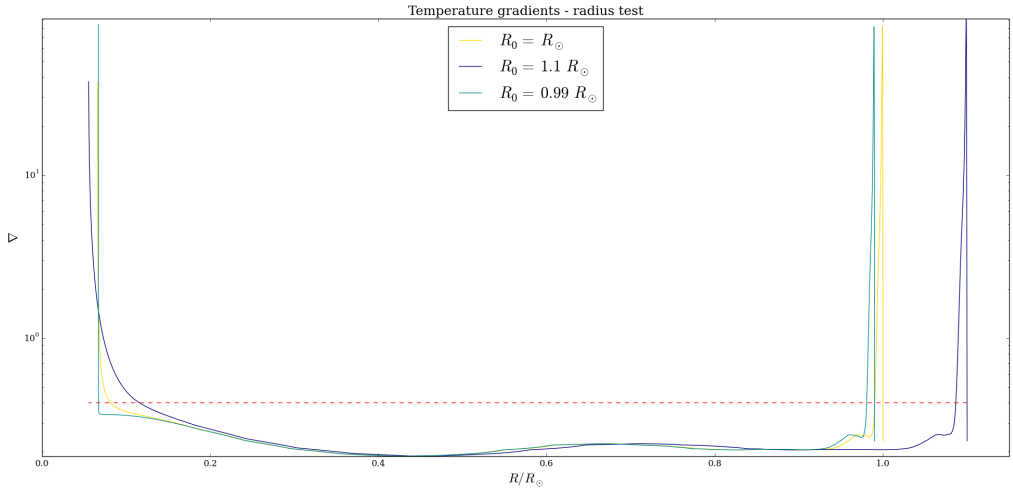

Figure 3: Test of the initial values of radius, equal $R_\odot$, 1.1 $R_\odot$, 0.99 $R_\odot$. Plot shows the temperature gradients (dashed line: ∇_{ad}, solid line: ∇_{stable}).

3.2 Best model

By making of the knowledge acquired throughout tests with various initial values, we decide to start with higher density, in order to reach the goal of width of the outer convection zone being at least 15% of R_0. Other parameters are being adjusted, so that we get around possible numerical problems. Keeping in mind that L_0 and M_0 are being kept unchanged, we decrease the radius while increasing the density, as well as adjust the temperature accordingly. In order to reach the other goals (L, M and R convergence), we apply the strategy that has been thoroughly decribed in the project one, taking into account the fact that the process of calculating temperature has been altered to include the energy transport by convection.

The initial parameters that have been found for the best model are:
$\rho_0 = 217\rho_{\odot,S} \approx 4.34 \cdot 10^{-2} \frac{\text{kg}}{\text{m}^3}$, $T_0 = 1.4\, T_{\odot,S} = 8078$ K and $R_0 = 0.84\, R_\odot \approx 5.92 \cdot 10^8$m.

The goal of convergence within the range of $0-5\%$ of initial values is reached, as the final mass is equal to 0.01% of M_0, final radius is equal to 4.9% of R_0 and final luminosity is 4.8% of L_0. See figure 6 for the behaviour of these parameters, as well as pressure, density and temperature as the function of radius.

Total energy production (divided by its maximal value) has been plotted, togehter with the fractions of energy production from each of the three PP-chain branches, as seen on figure 4. The fractions of energy being transported by convection, $F_C/(F_C + F_R)$, and radiation, $F_R/(F_C + F_R)$, have also been plotted, see figure 5.

We have created the model of a star that has the core, where luminosity is smaller than 0.995 L_0, reaching out to 29.7% of initial radius (so well above the required 10%). When it comes to the energy transport - the outer continous convection layer is of width 19.4% of initial radius ($> 15\%$, which was the goal), the outer radiation layer of width 49.9% of R_0, the inner radiation layer of width 20.4% of R_0 and the inner convection layer of width 4.2% of R_0 (adding these percentage results gives a bit less than 100% of R_0, since the convergence of radius is not completely to zero). The layers are marked on the cross-section plot in figure 7.

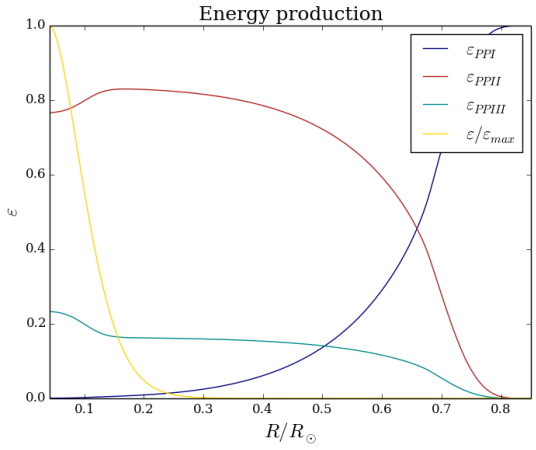

Figure 4: The total energy production divided by its maximum value, $\varepsilon/\varepsilon_{max}$, plotted together with the relative energy production from each of the three branches of PP-chain.

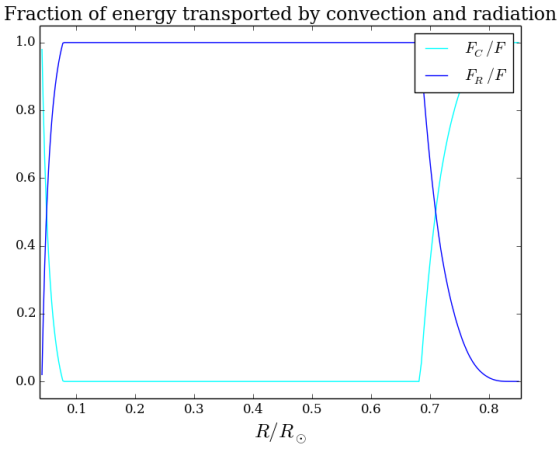

Figure 5: The fractions of energy being transported by convection, F_C/F, and radiation, F_R/F, as a function of radius.

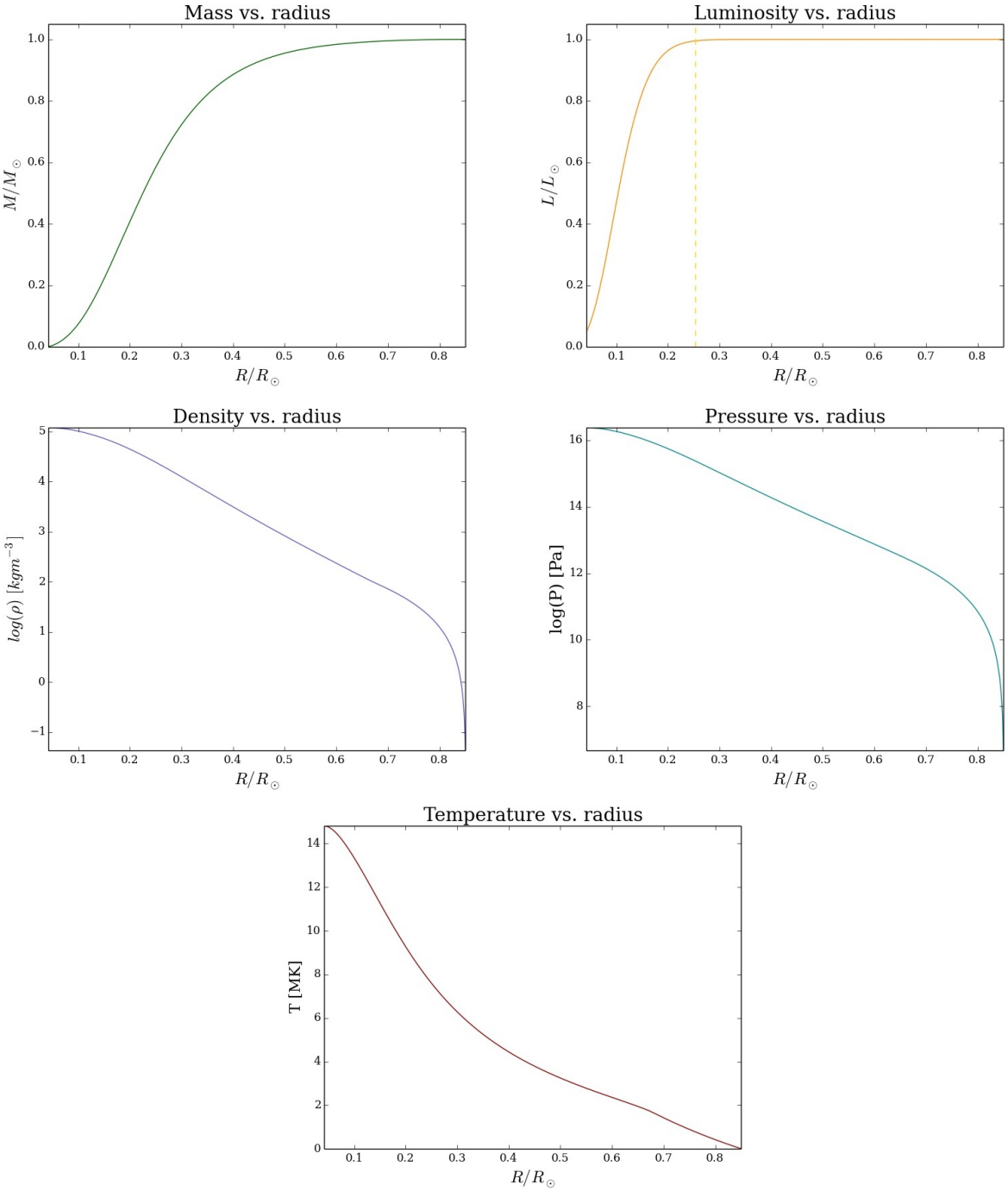

Figure 6: The behaviour of mass, luminosity, density and pressure as the function of radius. Vertiacal dashed line on the luminosity plot marks beginning of the core.

Last but not least, we have plotted the tempeature gradients, ∇^*, ∇_{stable} and ∇_{ad} as functions of radius (figure 8a), as well as the zoom on the outer convection layer (figure 8b).

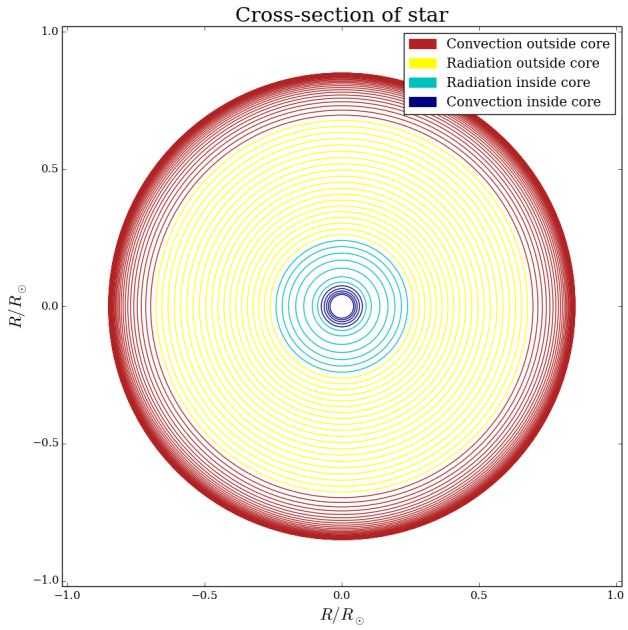

Figure 7: Cross-section of the best model of the star. The layers of energy transport by convection and radiation are marked on the plot.

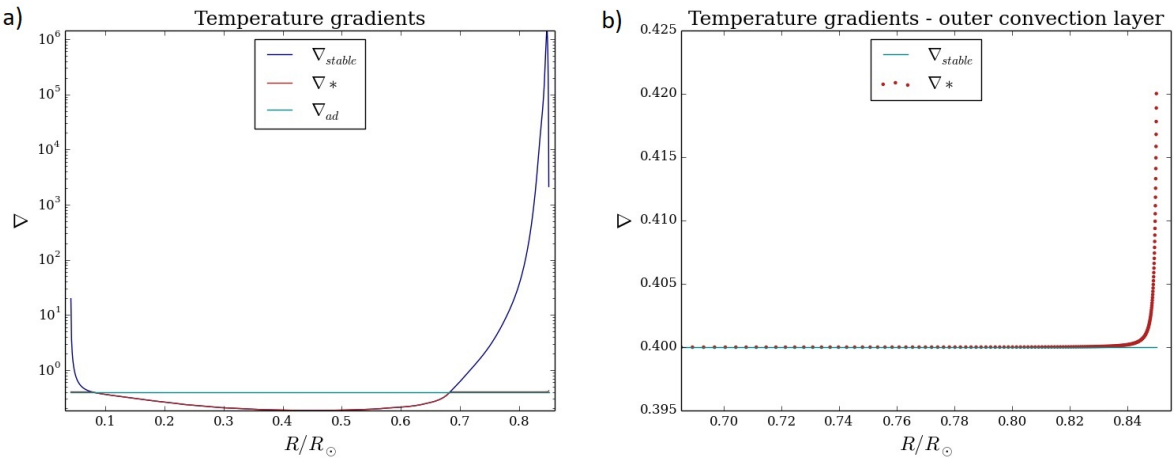

Figure 8: a) Temperature gradients of the best model, where $\nabla_{stable} > \nabla_{ad}$ marks the convection zone. b) Zoom on the outer convection layer.

4 Discussion and conclusions

4.1 Analysis of experiments with various initial values

The convection layer is associated with ∇_{stable} being larger than the constant ∇_{ad}. As long as this instability criterion holds, we are in the convection zone. The expression for ∇_{stable}

is given in the equation (8). Setting in the pressure scale height, H_p, with the gravitational acceleration, g, we have that $\nabla_{stable} \propto \frac{\kappa\rho L}{T^3 M}$. That implies that we get the wider convection zone if the temperature is increasing more slowly (this is important as we have T^3 in the expression) and mass decreasing faster, as well as the density increasing faster and luminosity decreasing more slowly. The impact of initial parameters on that behaviour was investigated in detail in the project one, but then with different calculation for the temperature. Now, applying the new algorithm for calculating the temperature change in the convection zone, we have $\frac{\partial T}{\partial m} = -\frac{T}{H_p}\nabla_{stable}\frac{\partial r}{\partial m} \propto -\frac{\kappa L}{r^4 T^3}$. Now we see that the temperature in the convection zone is clearly increasing much faster if the radius is dropping faster (lower r^4 gives big $|\frac{\partial T}{\partial m}|$). From the project one, we know that the parameter that has a big impact of behaviour of radius as the function of mass is initial density - very low initial density gave quickly dropping radius. Now, we want the radius to converge to zero more slowly, in order for the temperature to increase more slowly and hence, ∇_{stable} being larger than ∇_{ad} longer, which gives wider convection zone. To achieve that, we have to implement larger initial density, which is in agreement with the performed tests (see figure 1). Also, as seen on figure 2 and figure 3, other two tested initial parameters have not such a big impact on the width of the convection zone, but nevertheless their proper adjustment plays a key role in achiving the other goals, by applying the strategy from project one.

4.2 Analysis of best model and comparison with the Sun

The cross-section of the Sun is characterized by the core reaching out to 0.25 $R_\odot$, radiative zone reaching out to about 0.7 $R_\odot$ and the outer convection zone close to the solar surface. This gives the width of the outer radiative zone of 0.45 $R_\odot$, as well as the width of the outer convection zone of about 0.3 $R_\odot$. Our best model star has a little bit bigger core relatively to its radius, namely close to 0.3 R_0 (measured from the center, $R = 0$). Moreover, our radiative layer outside the core has width 0.5 R_0, so again slightly bigger, whereas the outer convection layer is not so wide as Sun's, relatively to its radius, with the width of 0.2 R_0. In general, the proportions between the layer sizes and their location in the cross-section are similar - we observe a core, then a wide radiative zone, and then a thinner convective zone for both stars (see figure 7).

The convective zones are associated with the energy transport mostly by convection, here $F_C > F_R \geq 0$, as can be observed on figure 5. Parts of the star, where the energy is transported entirely through radiation (outer and inner radiative layers) are also seen on the figure, here $F_R/F = 1$ and $F_C/F = 0$. From the temperature gradients plotted on figure 8a, we see that for convection zones $\nabla_{stable} > \nabla_{ad}$ (fulfilled instability criterion) and for radiative part $\nabla^* = \nabla_{stable} < \nabla_{ad}$. Figure 8b shows the zoom on the outer convection layer, with clearly visible behaviour of ∇^*.

On the figure 5, we have plotted the total energy production divided by its maximum value, which nicely shows that the vast majority of energy production happens inside the core (that reaches to about 0.3 $R_0 \approx 0.25$ $R_\odot$). This is in agreement with the luminosity plot from figure 6, as $\frac{\partial L}{\partial m} = \varepsilon$ (a change in mass is negative, so greater energy production $\Rightarrow$ faster dropping luminosity). Furthermore, we see that the relative energy production from PPI branch is dominating at low temperatures (for bigger radius), while PPII and PPIII is clearly dominating at higher temperatures, closer to the center, here $\varepsilon_{PPII} > \varepsilon_{PPIII} > \varepsilon_{PPI}$. This is also one of the established goals, that has been reached.